INTERNATIONAL JOURNAL FOR NUMERICAL METHODS IN FLUIDS
Int. J. Numer. Meth. Fluids 2009; **61**:341–354
Published online 2 December 2008 in Wiley InterScience (www.interscience.wiley.com). DOI: 10.1002/fld.1972

Shan-and-Chen-type multiphase lattice Boltzmann study of viscous coupling effects for two-phase flow in porous media

Haibo Huang*,†, Zhitao Li, Shuaishuai Liu and Xi-yun Lu

Department of Modern Mechanics, University of Science and Technology of China, Hefei, Anhui 230026, China

SUMMARY

In this paper, the Shan–Chen-type (SC) multiphase lattice Boltzmann model was used to study the viscous coupling effects for immiscible two-phase flow in porous media. In the model, any typical equation of state can be incorporated and different contact angles of the gas–liquid interface at a solid wall can be obtained easily through adjusting the 'density of wall' (Benzi *et al.*, *Phys. Rev. E* 2006; **74**(2):021509). The viscous coupling effects due to capillary number, the viscosity ratio and the wetting angle were investigated. The two-phase flows with density ratio as high as *56* in porous media were simulated. For different viscosity ratios and wettability, two-phase flow patterns and relative-permeability curves as a function of wetting saturation were obtained. It is observed that when the wetting phase is less viscous and covers the solid surface, the relative permeability of the non-wetting phase may be greater than unity. Here, the SC model is demonstrated as a suitable tool to study the immiscible two-phase flow in porous media because it is simple, easy to get the desired contact angle and able to simulate immiscible phase flow with high-density ratio. Copyright © 2008 John Wiley & Sons, Ltd.

Received 22 August 2008; Revised 19 October 2008; Accepted 26 October 2008

KEY WORDS: lattice Boltzmann; two-phase flow; relative permeability; Shan–Chen; viscous coupling; immiscible

1. INTRODUCTION

1.1. Lattice Boltzmann for multiphase flow

The lattice Boltzmann method (LBM), which is based on mesoscopic kinetic equations, has become a promising numerically robust technique for simulating multi-phase fluids [1–5]. Compared with conventional methods for multiphase flows, LBM does not track interfaces while sharp interfaces

*Correspondence to: Haibo Huang, Department of Modern Mechanics, University of Science and Technology of China, Hefei, Anhui 230026, China.
†E-mail: huanghb@ustc.edu.cn

Contract/grant sponsor: National Science Foundation of China (NSFC); contract/grant number: 10802085

can be maintained automatically [3]. LBM has been successfully applied to study wetting and spreading phenomena [6–11], bubble collision and bubble rising phenomena [3, 4], displacement of immiscible fluids in porous media [2, 12–16], etc.

There are several popular multiphase models in LBM. The first type is the color-gradient-based LBM proposed by Gunstensen *et al*. [17], which is based on the Rothman–Keller lattice gas model [18]. The second type is the original Shan–Chen (SC) model [1]. The third type is free-energy-based LBM [19]. The multiphase model proposed by He *et al*. [20], which uses the idea of level set, is also very popular.

Although LBM has made great progress in multiphase flow modeling, all the above LBMs are limited to small density ratios less than 10 because numerical instability may appear in cases of large density ratio. Inamuro *et al*. [3] and Lee and Lin [21] achieve a high-density ratio through improving Swift's free-energy model [19] and the model of He *et al*. [20] respectively. However, both of their models uses two sets of particle distribution functions (PDF) that undermine the simplicity of the LBM or increase computational loads. Recently, it has been found that through using just one set of PDF, different equations of state (EOS) can be incorporated into the SC LBM so as to achieve high-density ratio [22]. The surface tension for different EOS in SC LBM can be determined analytically [8, 23].

Yiotis *et al*. applied the multiphase model of He *et al*. [20] to study the immiscible two-phase flow in porous media and obtained some results [14]. However, in the model of He *et al*. [20], the surface tension has to be obtained through finite difference method, a special treatment may be necessary to handle the solid walls. Besides this inconvenience, two sets of PDF used in simulations will increase computational loads and high-density-ratio two-phase flow is very difficult to realize. Pan *et al*. [12] and Li *et al*. [13] applied SC two-component multiphase LBM to study the two-component flow in porous media. However, when using the SC two-component multiphase LBM, the viscosity ratio M is around 1 due to numerical instability and the maximum M in their study is only about 3.

As mentioned above, the revised single-component multiphase SC LBM [22] can incorporate different EOS into the model and high-density-ratio two-phase flow can be achieved. On the other hand, the wettability at solid–fluid interfaces about this model was fully studied by Benzi *et al*. [8] and different contact angles of the fluid–fluid interface at a solid wall can be obtained by adjusting the 'density of wall' conveniently [8]. Here, we will focus on the SC LBM exclusively.

In this paper, the single-component multiphase SC LBM would be applied to study the high-density-ratio two-phase flow in porous media, so as to test this model's performance on this topic. At the same time, the viscous coupling effects due to capillary number, the viscosity ratio and the wetting angle would be investigated in detail.

1.2. Two-phase flow in porous media

It is well known that the isotropic flow of a Newtonian fluid through a porous medium can be described by Darcy's law $u = -k\Delta p/\mu l$, where u is the average velocity of the fluid at inlet or outlet boundary, $\Delta p/l$ is the pressure gradient, μ is the viscosity of the fluid, k is the permeability which only depends on the geometry of the porous media.

For multiphase flows in porous media, a typical situation is that the wetting phase covers the solid surface and moves along the surface, while the non-wetting phase flows in the center of the pores, surrounded by the wetting fluid. Hence, there is strong viscous coupling between the wetting and non-wetting fluids [14].

DOI: 10.1002/fld

To account for momentum transfer across fluid–fluid interfaces and viscous coupling effects, through defining an apparent relative permeability $k_{r,i}$ which is a function of S_w, Ca and M, Darcy's law may be modified as [14] $u_i = -kk_{r,i}(S_w, Ca, M, \Delta p_i)\Delta p_i/\mu l$, where i indicates 'wetting' or 'non-wetting' phase, S_w is the wetting saturation, $Ca = u_w\mu_w/\sigma$ is the capillary number and $M = \mu_{nw}/\mu_w$ is the viscosity ratio.

In this paper, we first briefly review the SC single-component multiphase LBM. Then SC LBM code was validated by verifying the velocity profile for two-phase flow through a 2D channel. After that the multiphase flow in porous media with different viscosity ratios, capillary number, wettability were simulated. Finally, the flow patterns and relative permeabilities of two phases were investigated.

2. METHOD

2.1. Shan-and-Chen-type single-component multiphase LBM

Here we implement the SC LBM [1] in two dimensions for a single-component multiphase system. In the model, one distribution function is introduced for the fluid. The distribution function satisfies the following lattice Boltzmann equation:

$$f_a(\mathbf{x}+\mathbf{e}_a\Delta t, t+\Delta t) = f_a(\mathbf{x}, t) - \frac{\Delta t}{\tau}(f_a(\mathbf{x}, t) - f_a^{\mathrm{eq}}(\mathbf{x}, t)) \tag{1}$$

where $f_a(\mathbf{x}, t)$ is the density distribution function in the ath velocity direction and τ is a relaxation time that is related to the kinematic viscosity as $v = c_s^2(\tau - 0.5\Delta t)$. In the SC LBM, the effect of body force is incorporated through adding an acceleration into velocity field. The equilibrium distribution function $f_a^{\mathrm{eq}}(\mathbf{x}, t)$ can be calculated as

$$f_a^{\mathrm{eq}}(\mathbf{x}, t) = w_a\rho\left[1 + \frac{\mathbf{e}_a\cdot\mathbf{u}^{\mathrm{eq}}}{c_s^2} + \frac{(\mathbf{e}_a\cdot\mathbf{u}^{\mathrm{eq}})^2}{2c_s^4} - \frac{(\mathbf{u}^{\mathrm{eq}})^2}{2c_s^2}\right] \tag{2}$$

In Equations (1) and (2), the $\mathbf{e}_a$s are the discrete velocities. For the D2Q9 model, they are given by

$$[\mathbf{e}_0, \mathbf{e}_1, \mathbf{e}_2, \mathbf{e}_3, \mathbf{e}_4, \mathbf{e}_5, \mathbf{e}_6, \mathbf{e}_7, \mathbf{e}_8] = c\cdot\begin{bmatrix} 0 & 1 & 0 & -1 & 0 & 1 & -1 & -1 & 1 \\ 0 & 0 & 1 & 0 & -1 & 1 & 1 & -1 & -1 \end{bmatrix}$$

In Equation (2), for the D2Q9 model, $w_a = \frac{4}{9}$ $(a=0)$, $w_a = \frac{1}{9}$, $(a=1,2,3,4)$, $w_a = \frac{1}{36}$, $(a=5,6,7,8)$, $c_s = c/\sqrt{3}$, where $c = \Delta x/\Delta t$ is the ratio of lattice spacing Δx and time step Δt. Here, we define 1 lattice unit (Δx) as 1 lu. In Equation (2), ρ is the density of the fluid, which can be obtained from $\rho = \sum_a f_a$.

The macroscopic velocity $\mathbf{u}^{\mathrm{eq}}$ is given by

$$\mathbf{u}^{\mathrm{eq}} = \mathbf{u}' + \frac{\tau\mathbf{F}}{\rho} \tag{3}$$

where $\mathbf{u}'$ is the velocity defined as

$$\mathbf{u}' = \frac{\sum_a f_a\mathbf{e}_a}{\rho} \tag{4}$$

DOI: 10.1002/fld

In Equation (3), $\mathbf{F}=\mathbf{F}_{\text{int}}+\mathbf{F}_{\text{ads}}+\mathbf{F}_{\text{ext}}$ is the force acting on the fluid, here including the inter-particle force $\mathbf{F}_{\text{int}}$, adhesion force between liquid/gas phase and solid phase and external force $\mathbf{F}_{\text{ext}}$. In this study $\mathbf{F}_{\text{ext}}$ is a uniform steady body force. The whole fluid velocity $\mathbf{u}$ is defined as:

$$\mathbf{u}=\mathbf{u}'+\frac{\mathbf{F}}{2\rho} \tag{5}$$

The inter-particle force is defined as [2],

$$\mathbf{F}_{\text{int}}(\mathbf{x},t)=-g\psi(\mathbf{x},t)\sum_a w_a\psi(\mathbf{x}+\mathbf{e}_a\Delta t,t)\mathbf{e}_a \tag{6}$$

where g is a parameter that controls the strength of the inter-particle force. For the EOS proposed by Shan and Chen [1],

$$\psi(\rho)=\rho_0[1-\exp(-\rho/\rho_0)] \tag{7}$$

where ρ_0 is a constant.

Through Taylor expanding as described in Appendix A in Reference [23] and $-\partial_j p+\partial_i(c_s^2\rho)=F_i$, we can obtain [23]:

$$p=c_s^2\rho+\frac{c_s^2 g}{2}\psi^2 \tag{8}$$

According to the Yuan and Schaefer [22], if the EOS of $p=p(\rho)$ is already known, we can use following formula:

$$\psi=\sqrt{\frac{2(p-c_s^2\rho)}{c_s^2 g}} \tag{9}$$

to incorporate different EOS into the SC LBM.

The typical EOS are the van der Waals, Redlich-Kwong, Redlich-Kwong Soave, Peng-Robinson and Carnahan-Starling equation. They are given out in detail in Reference [22]. The surface tension was calculated through Laplace Law after the equilibrium state was obtained in LBM simulations. Analytical solutions of surface tension for these EOS can also be conveniently obtained through solving equations in Reference [23].

The desired contact angle can also be obtained conveniently through change in parameter ρ_{w} [8]. The adhesion force between gas/liquid phase and solid walls is calculated by the following equation, where we assume the density of solid phase is ρ_{w}, i.e. $\psi(\rho(x_{\text{w}}))=\psi(\rho_{\text{w}})$,

$$\mathbf{F}_{\text{ads}}(\mathbf{x},t)=-g\psi(\rho(\mathbf{x},t))\sum_a w_a\psi(\rho_{\text{w}})s(\mathbf{x}+\mathbf{e}_a\Delta t,t)\mathbf{e}_a \tag{10}$$

Here $s(\mathbf{x}+\mathbf{e}_a\Delta t,t)$ is an indicator function that is equal to 1 or 0 for a solid or a fluid domain node, respectively. ρ_{w} is not really relevant to the 'true' density of solid phase, it is a free parameter used here to tune different wall properties [8].

In our simulations, any lattice node in the computational domain represents either a solid node or a fluid node. For the solid node, before streaming step, the bounce-back algorithm and not the collision step is implemented to mimic non-slip wall boundary condition.

Figure 1 demonstrates that different contact angles can be obtained through adjusting ρ_{w}. In these simulations, the computational domain is 200×100, the upper and lower boundary is solid walls

DOI: 10.1002/fld

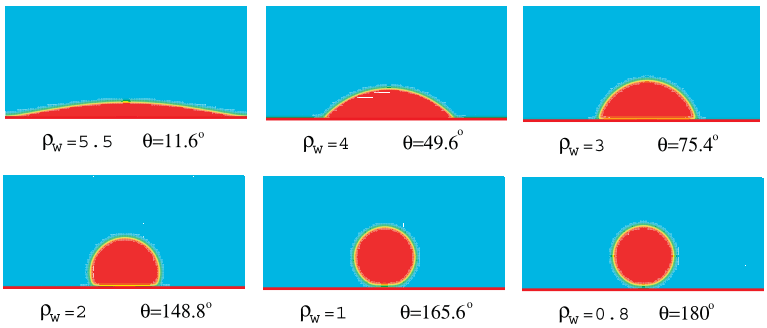

Figure 1. Different contact angles obtained through adjusting the parameter ρ_w. R-K EOS was used in the simulations.

and the east and west boundary is periodic. The EOS used in the LB simulation is Edlich-Kwong ($\mathbf{R}-K$) EOS:

$$p=\frac{\rho RT}{1-b\rho}-\frac{a\rho^2}{\sqrt{T}(1+b\rho)} \tag{11}$$

with $a=\frac{2}{49}$, $b=\frac{2}{21}$, $T_c=0.1961$ and $T=0.85T_c$. The liquid phase density is $\rho_l=6.06$ and gas phase density is $\rho_g=0.5$. When the parameter ρ_w varies between ρ_l and ρ_g, the contact angle varies between 0 and 180°. The surface tension can be obtained analytically [23] and the value of surface tension is adjustable through change parameter b in the EOS.

3. RESULTS AND DISCUSSION

3.1. Viscous coupling in co-current flow in a 2D channel

For immiscible two-phase flows in porous media, a typical situation is that the wetting fluid attaches and moves along the solid surface, while the non-wetting phase flows in the center of the pores. The velocity of the non-wetting phase is relevant to the viscosity ratio of the non-wetting and wetting fluids, i.e. $M=\mu_{nw}/\mu_w$.

Here we studied the immiscible two-phase co-current flow through two parallel plates. In the simulation, the periodic boundary condition was applied in the inlet/outlet boundary. Non-slip (bounce-back) boundary conditions were applied in the upper and lower plates. The kinematic viscosity for non-wetting and wetting fluid are $v_{nw}=v_w=c_s^2(\tau-0.5)$, Hence $M=\rho_{nw}/\rho_w$.

In the simulation, as illustrated in Figure 2, the wetting phase flows in the region $a<|y|<b$, and the non-wetting phase flows in the central region $0<|y|<a$. Obviously, the saturation of wetting fluid in this study is $S_w=1-a/b$, and $S_{nw}=a/b$. Assuming a Poiseuille-type flow in the channel, the analytical solution for the velocity profile between the parallel plates is [14]

$$u(y)=\frac{\Delta p}{2l\mu_w}(b^2-y^2)=\frac{\Delta F}{2\mu_w}(b^2-y^2) \tag{12}$$

DOI: 10.1002/fld

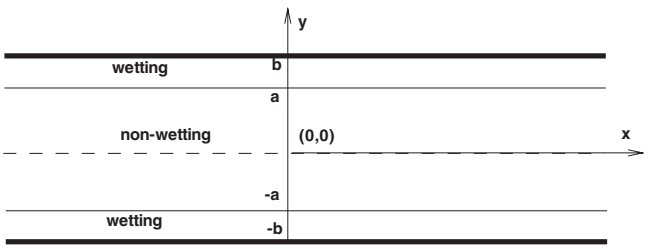

Figure 2. Co-current immiscible two-phase flow in a 2D channel, the wetting phase flows along the upper and lower plate while non-wetting phase flows in the center region.

in the wetting region, $a<|y|<b$, and

$$u(y)=\frac{\Delta F}{2\mu_{\mathrm{w}}}(b^2-a^2)+\frac{\Delta F}{2\mu_{\mathrm{nw}}}(a^2-y^2) \tag{13}$$

in the non-wetting fluid region, $0<|y|<a$.

In above equations, the pressure gradient in the direction of the flow is taken equal to ΔF. The ΔF can be directly incorporated into the force $\mathbf{F}$ in the Equation (3).

Using Equations (12) and (13), the relative permeability of each phase as a function of the wetting saturation can be obtained as [14]

$$\begin{aligned} k_{\mathrm{r,w}} &= \tfrac{1}{2}S_{\mathrm{w}}^2(3-S_{\mathrm{w}}) \\ k_{\mathrm{r,nw}} &= S_{\mathrm{nw}}[\tfrac{3}{2}M+S_{\mathrm{nw}}^2(1-\tfrac{3}{2}M)] \end{aligned} \tag{14}$$

From Equation (14), we can see that the $k_{\mathrm{r,w}}\in[0,1]$ when $S_{\mathrm{w}}\in[0,1]$, while the $k_{\mathrm{r,nw}}$ may be higher than 1 when $S_{\mathrm{w}}\in[0,1]$ because $k_{\mathrm{r,nw}}$ is not only a function of S_{w} but also M.

For the cases $M<1$, Figure 3 shows the velocity profile for $M=0.0833$ and $S_{\mathrm{w}}=0.333$. The velocity profile calculated from LBM agrees with the analytical one. Figure 5 illustrates the $k_{\mathrm{r,nw}}$ and $k_{\mathrm{r,w}}$ as a function of the S_{w} when $M<1$. Again, the LBM results agree well with the analytical curves. As expected in Equation (14), relative permeabilities of both phases are smaller than 1.

For the cases $M>1$, Figure 4 shows the velocity profile for $M=12$ and $S_{\mathrm{w}}=0.75$. Overall the velocity profile obtained from LBM also agrees well with the analytical one. The non-wetting-phase velocity obtained from LBM is slightly higher than that of analytical one and in the vicinity of interface there is a small velocity jump. That may due to the interface force between the two phases. Figure 6 illustrates the $k_{\mathrm{r,nw}}$ and $k_{\mathrm{r,w}}$ as a function of the S_{w} when $M>1$. The LBM result is very consistent with the analytical solution. From the figure, we can see that the $k_{\mathrm{r,nw}}$ is greater than unity for most S_{w} values. That means the non-wetting phase flow flux is larger than 100%-non-wetting-saturated case when $0<S_{\mathrm{w}}<0.925$. This is due to the 'lubricating' effect of the wetting fluid.

3.2. Two-phase flow through porous media

In this section, two-phase flow in a porous medium was simulated. Porous media structure generations are not a topic of concern here. The porous medium in our simulations is the same as that in Reference [14], which is represented by 2D pore networks of $20^2\,\mathrm{lu}^2$ (lattice unit) square solid

DOI: 10.1002/fld

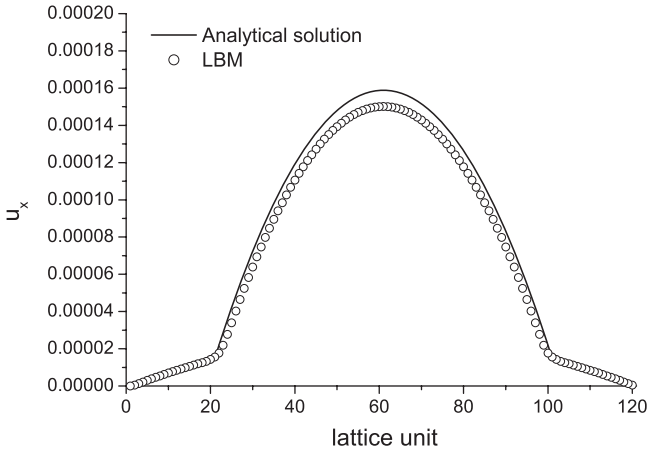

Figure 3. Velocity profile u_x in the middle of the 2D channel, the wetting phase is more viscous, $\Delta F = 1.5 \times 10^{-8}$, $v = 0.1667$, $M = 0.0833$.

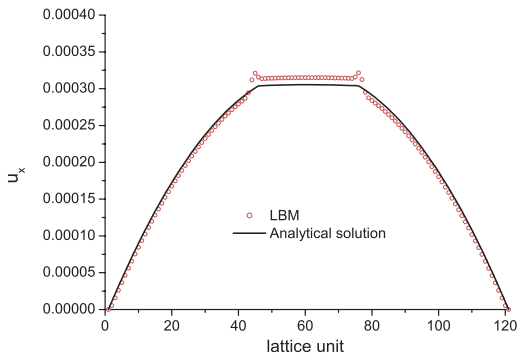

Figure 4. Velocity profile u_x in the middle of the 2D channel, the wetting phase is less viscous, $\Delta F = 1.5 \times 10^{-8}$, $v = 0.1667$, $M = 12$.

and void (pore space) blocks. The porosity of the network is $\varepsilon = 0.77$. The size of whole network is $400 \times 400\,\mathrm{lu}^2$.

Initially, the wetting phase and non-wetting phase were distributed randomly in the pores, i.e. wetting or non-wetting phase in each void blocks such that the desired wetting saturation was obtained.

In the simulations, periodic boundary conditions were applied in all directions. Co-current flow was simulated by adding body forces G for both phases along the flow direction because adding body phase is simple and is able to avoid capillary pressure gradients and thus saturating gradients along the flow direction [13]. The wetting and non-wetting phase flow fluxes were calculated at inlet and outlet during the simulations. If the relative flow flux difference between 1000 steps is less than 0.1%, it is assumed that the final steady state is reached.

DOI: 10.1002/fld

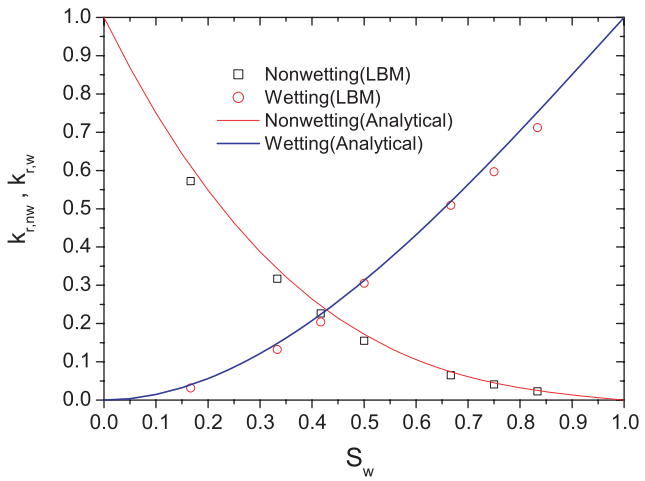

Figure 5. Relative permeabilities for the wetting phase ($k_{\mathrm{r,w}}$) and non-wetting phase ($k_{\mathrm{r,nw}}$) as a function of wetting saturation for co-current flow in a 2D channel. $M=0.0833$.

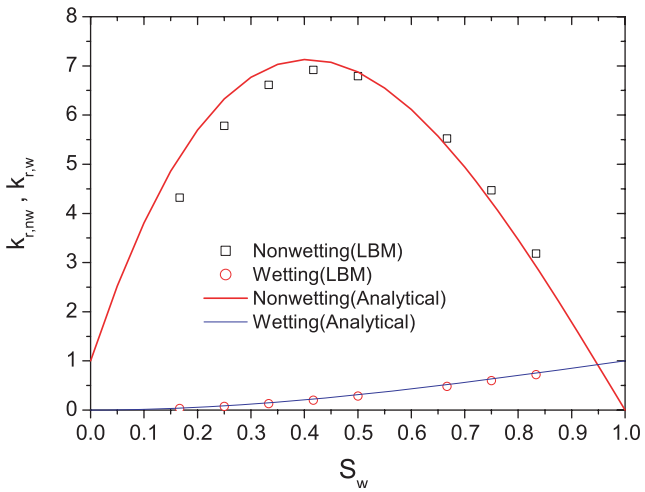

Figure 6. Relative permeabilities for the wetting phase ($k_{\mathrm{r,w}}$) and non-wetting phase ($k_{\mathrm{r,nw}}$) as a function of wetting saturation for co-current flow in a 2D channel. $M=12$.

It is well known that three non-dimensional parameters are important for the immiscible two-phase flow through porous media. These parameters are viscosity ratio M, Reynolds number $Re=ud/v$ and capillary number $Ca=u\mu/\sigma$.

In all of our simulations, the kinematic viscosity is $v=1/3(\tau-0.5)=0.1667$. The maximum gas velocity in our simulations was $u=0.2\,(\mathrm{lu/ts})$ in the porosity 2D pore networks in 100%-gas-saturated flow. The maximum Reynolds number in our simulations was $Re=u\times 20/v=24$. Here we assumed the Darcy's law is valid in all of the cases we studied.

DOI: 10.1002/fld

Figure 7. Steady-state two-phase distribution patterns in the cases of $S_w=0.2$, $S_w=0.5$ and $S_w=0.8$ when $Ca=6.25\times10^{-5}$, $M=12$, $\theta=180°$. In the LBM simulation, R-K EOS was used, $\sigma=0.16$. The wetting phase is shown in light gray. The non-wetting phase is shown in dark gray and the solid surface is black: (a) $S_w=0.2$; (b) $S_w=0.5$; and (c) $S_w=0.8$.

Ca can be regarded as the ratio of the body forces to the interfacial forces [14]. In the following simulations, we used R-K EOS, $M=12$ and the applied body force in our simulations was $G=10^{-5}$ or $G=10^{-4}$. The corresponding capillary numbers are $Ca=G/\sigma=10^{-5}/0.16=6.25\times10^{-5}$ and 0.000625, respectively. These are relatively high values of Ca, where the movement of the interface is controlled by viscous forces.

Figure 7 shows the steady two-phase distribution patterns in the cases of $S_w=0.2$, $S_w=0.5$ and $S_w=0.8$ when $Ca=6.25\times10^{-5}$. It is a strong wetting case when $\rho_w=0.5$ and $\theta=180°$. In the figure, the wetting phase is shown in light gray. The non-wetting phase is shown in dark gray and the solid surface is shown in black.

Figure 7(a) shows when $S_w=0.2$, the wetting phase is discontinuous and covers the solid surface, while the non-wetting phase is continuous and flows through the porous media. The wetting phase is practically immobile and $k_{r,w}=0$. The relative permeability of non-wetting phase is about 1.3 because the non-wetting phase flows among the wetting phase films and takes the advantage of the lubricating effect.

Figure 7(b) shows that the phase distribution pattern of the case $S_w=0.5$. The non-wetting phase is continuous and wetting phase is disconnected by the non-wetting phase.

For the case of $S_w=0.8$, as demonstrated in Figure 7(c), the non-wetting phase forms several large blobs and is discontinuous. These blobs are trapped in big pores due to the resistance of the capillary force and are immobile.

The relative permeabilities $k_{r,nw}$ and $k_{r,w}$ as a function of S_w is shown in Figure 8. Owing to the lubricating effect, the $k_{r,nw}$ is larger than unity when $0<S_w<0.4$ for cases of $Ca=6.25\times10^{-5}$. It is also found that the curves of relative permeabilities are not smooth. One of the possible reasons is that due to the randomness of structure, the specified phase randomization at the initial state may slightly affect the final steady phase distribution and hence the value of relative permeabilities. The spurious velocity [22] near the interface area may also affect the accuracy of flow flux calculation in the inlet and outlet boundary. How to reduce such fluctuation or estimate the fluctuation's value is a research topic in a following paper.

3.2.1. Effect of capillary number. The influence of Ca on the conventional relative permeabilities is shown in Figure 8. Relative-permeability curves for two Ca's $Ca=6.25\times10^{-5}$ and

DOI: 10.1002/fld

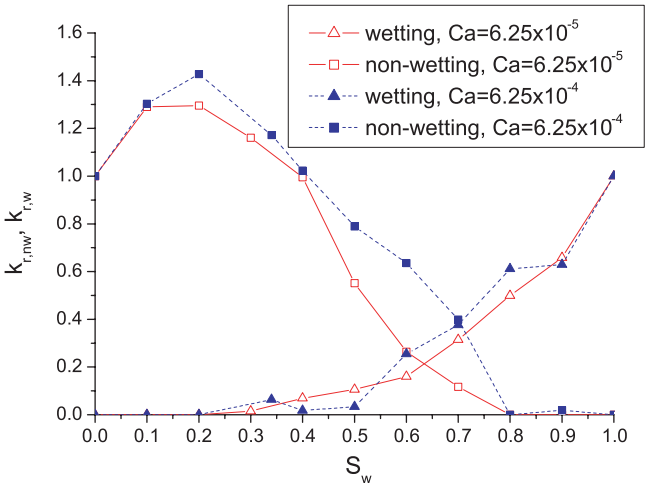

Figure 8. Relative permeabilities for the wetting phase ($k_{r,w}$) and non-wetting phase ($k_{r,nw}$) as a function of wetting saturation for co-current two-phase flow in a 2D porous. $M=12$, $\theta=180°$. R-K EOS was applied in the LB simulation, $\sigma=0.16$.

$Ca=6.25\times10^{-4}$ were compared. It is found that both the relative permeabilities for the two phases are increasing functions of Ca for the fluid system when $M=12$ and $\theta=180°$. This trend was also observed by Li *et al.* [13] numerically although in their study $M=1$.

3.2.2. Effect of wettability. In this section, the dependence of the relative permeability on wettability was studied. Neutrally wet cases were also discussed in this subsection. For the neutrally wet media, the $\rho_w=2.0$, the contact angle for the more viscous phase is 148.8°. The capillary number is $Ca=6.25\times10^{-5}$.

In the neutrally wet porous media, steady-state two-phase distribution patterns for different S_w are illustrated in Figure 9. Comparing Figure 7(c) and Figure 9(c), it is observed that for $S_w=0.8$, the non-wetting phase has a smaller specific interfacial area with the solid phase, which means smaller resistance to flow, in the strongly wet media than in the neutrally wet media. For the other given S_w, the mechanism is also valid [13]. This mechanism seems dominant because in Figure 10, there are higher $k_{r,nw}$ in the strongly wet media than in the neutrally wet system.

In Figure 10, there are very small differences for neutrally wet and strongly wet systems in terms of $k_{r,w}$. As we know, at a given saturation level, non-wetting phase tends to occupy larger pores in a strongly wet media, so the wetting phase tends to occupy smaller pore space in the strongly wet media . This mechanism may make the $k_{r,w}$ lower in strongly wet media than in the neutrally wet media. On the other hand, the wetting phase seems more connected in strongly wet media, which may make the $k_{r,w}$ higher in strongly wet media [13]. While Figure 10 demonstrates that the net effect of these two off-setting mechanisms is a relatively small difference in $k_{r,w}$ as a function of S_w. The above results are consistent with the results of Li *et al.* [13].

When $\rho_w=4.0$, contact angle of more viscous phase is 49.6°. In these cases, the more viscous phase is wetting phase and $M=0.0833$. The body forces applied to the two phases are 10^{-5} and $Ca=6.25\times10^{-5}$. Steady-state two-phase-distribution patterns in the porous media for $S_{nw}=0.2$, $S_{nw}=0.5$ and $S_{nw}=0.8$ are illustrated in Figure 11.

DOI: 10.1002/fld

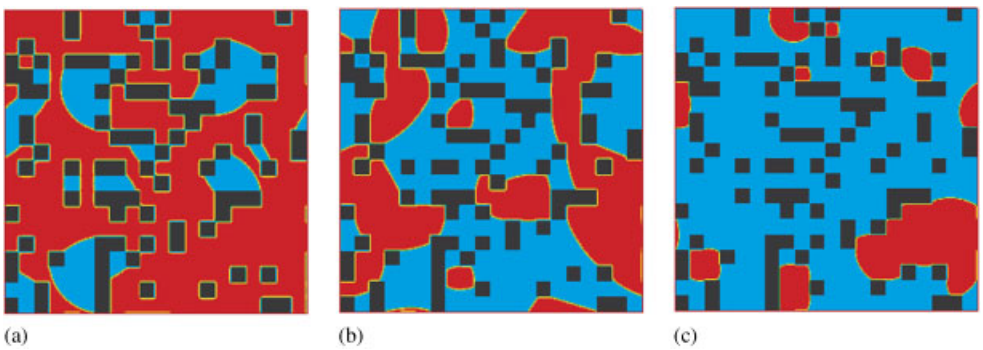

Figure 9. Steady-state two-phase distribution patterns in the cases of $S_w = 0.2$, $S_w = 0.5$ and $S_w = 0.8$ when $Ca = 6.25 \times 10^{-5}$. $M = 12$, R-K EOS was applied in the LB simulation, $\sigma = 0.16$, $\rho_w = 2.0$, $\theta = 148.8°$. The less viscous phase (wetting) is shown in light gray. The more viscous phase (non-wetting) is shown in dark gray and the solid surface is shown in black: (a) $S_w = 0.2$; (b) $S_w = 0.5$; and (c) $S_w = 0.8$.

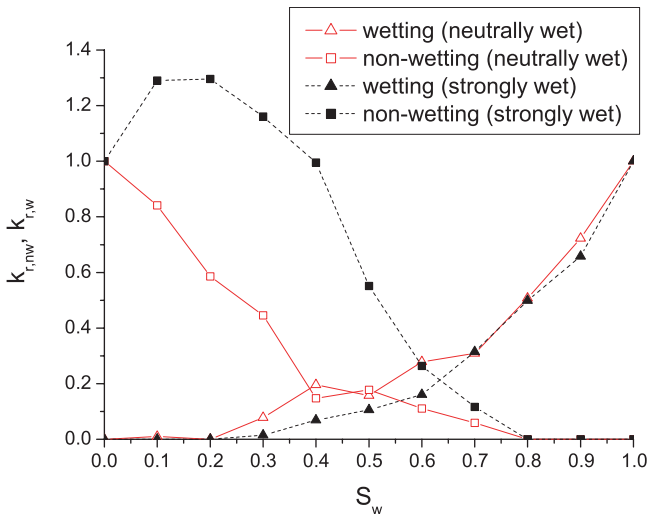

Figure 10. Relative permeabilities for the wetting phase ($k_{r,w}$) and the non-wetting phase ($k_{r,nw}$) as a function of wetting saturation for co-current two-phase flow in a 2D porous. $M = 12$, R-K EOS was applied in the LB simulation, $\sigma = 0.16$. For strongly wet cases, $\rho_w = 0.5$, $\theta = 180°$; for neutrally wet cases, $\rho_w = 2.0$ and $\theta = 148.8°$.

In the figure, for $S_{nw} = 0.2$ the wetting phase covers most of the solid walls and non-wetting phase forms three big blobs in the large pore area. For the case of $S_{nw} = 0.5$ and $S_{nw} = 0.8$, due to the solid wall's neutral-wetting property, both two phases are in contact with the solid wall. When $S_{nw} = 0.5$, it seems that the viscous wetting phase covers more solid surface. In this case, more big pores are filled by blobs compared with non-wetting phase in case $S_{nw} = 0.2$. When $S_{nw} = 0.8$, the non-wetting phase becomes continuous and the wetting phase is disconnected.

DOI: 10.1002/fld

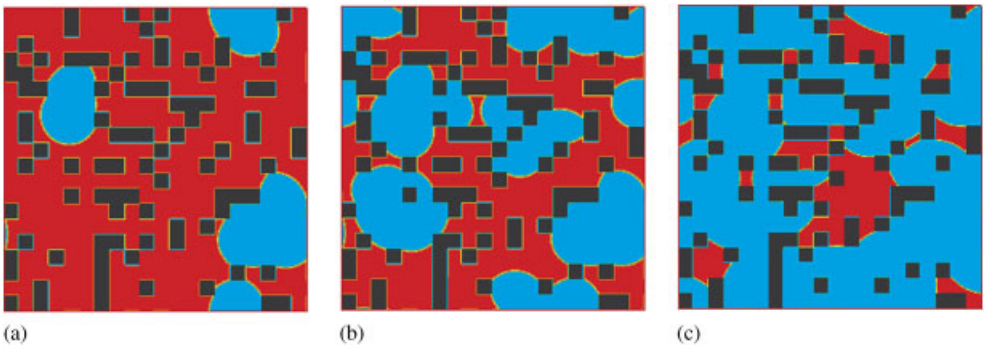

Figure 11. Steady-state two-phase distribution patterns in the cases of $S_{nw}=0.2$, $S_{nw}=0.5$ and $S_{nw}=0.8$ when $Ca=6.25\times10^{-5}$. $M=0.0833$, R-K EOS was applied in the LB simulation, $\sigma=0.16$, $\rho_w=4.0$, $\theta=49.6°$. The more viscous phase (wetting) is shown in dark gray. The less viscous phase (non-wetting) is shown in light gray and the solid surface is shown in black: (a) $S_{nw}=0.2$; (b) $S_{nw}=0.5$; and (c) $S_{nw}=0.8$.

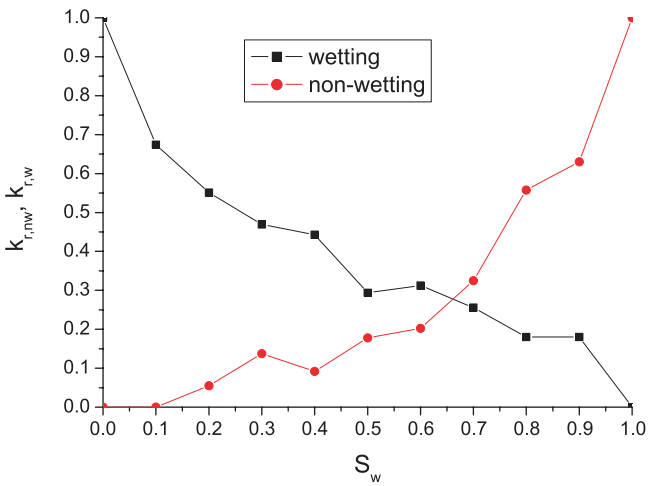

Figure 12. Relative permeabilities for the wetting phase ($k_{r,w}$) and non-wetting phase ($k_{r,nw}$) as a function of wetting saturation for co-current two-phase flow in a 2D porous. R-K EOS was applied in the LB simulation, $M=0.0833$, $\sigma=0.16$, $\rho_w=4.0$, $\theta=49.6°$.

Figure 12 shows the relative permeabilities as a function of S_w for $M=0.0833$ and $\theta=49.6°$. As expected, both the $k_{r,w}$ and $k_{r,nw}$ are less than 1 in whole S_w range.

3.2.3. Effect of viscosity ratio. Here we focus on the topic about how relative permeabilities depend on the viscosity ratio M of two phases.

To achieve higher density ratio, here in our LB simulations, the EOS used is Carnahan–Starling (**C–S**) EOS: $p=\rho RT(1+b\rho/4+(b\rho/4)^2-(b\rho/4)^3)/(1-b\rho/4)^3-a\rho^2$ with $a=1$, $b=4$,

DOI: 10.1002/fld

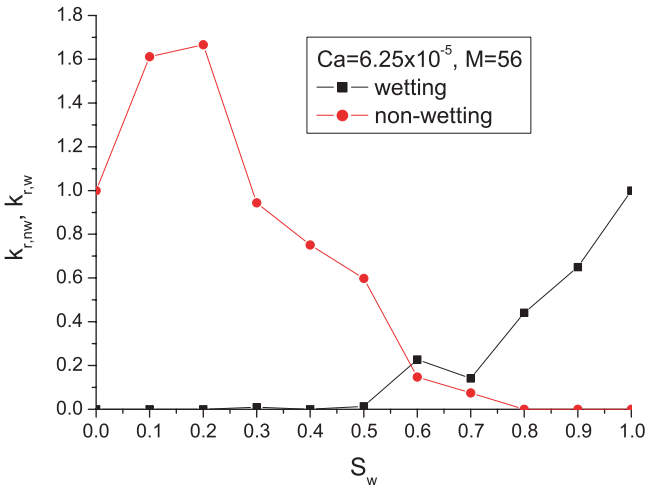

Figure 13. Relative permeabilities for the wetting phase ($k_{r,w}$) and non-wetting phase ($k_{r,nw}$) as a function of wetting saturation for co-current two-phase flow in a 2D porous. The C-S EOS was used in the simulations, $\rho_{liquid}=0.359$, $\rho_{gas}=0.00645$, $\sigma=0.0145$, $M=56$, $Ca=6.25\times10^{-5}$, $G=9.06\times10^{-7}$, $\theta=180°$.

$T_c=0.0943$ and $T=0.7T_c$, the liquid phase density is $\rho_l=0.359$ and gas phase density is $\rho_g=0.00645$. When the parameter ρ_w varies between ρ_l and ρ_g, the contact angle varies between 0 and 180°.

Figure 13 shows the relative permeabilities as a function of S_w for $M=56$. Compared with Figure 8, it is found that although Ca is same, increase of M makes $k_{r,nw}$ increase significantly, especially when the S_w is in the intermediate range. That is due to the 'lubricating' effect of the wetting phase film that attaches the wall. It also demonstrates that the greater the viscosity ratio M, the larger the 'lubricating' effect.

It is found that in cases of a higher M, there is more connected non-wetting phase pathway [13, 24], which may also contribute to the trend of $k_{r,nw}$ increasing with M.

On the other hand, the $k_{r,w}$ is not so sensitive to M. This can be observed clearly in Figures 8 and 13.

4. CONCLUSIONS

In this paper, the immiscible single-component two-phase flow in porous media was studied using Shan–Chen-type (SC) multiphase lattice Boltzmann model. Two-phase distribution patterns and relative permeability curves as a function of wetting saturation for different viscosity ratios and wettability were obtained. When $M>1$, the relative permeability of non-wetting phase may be greater than unity due to the lubricating effect. While when $M<1$, the $k_{r,nw}$ and $k_{r,w}$ are always less than 1.

Our study demonstrates that SC single-component multiphase LBM is a very good tool to study the immiscible two-phase flow in porous media due to its simplicity, capability of investigating wettability effect and achieving high-density-ratio two-phase flow.

DOI: 10.1002/fld

ACKNOWLEDGEMENTS

Huang was supported by National Science Foundation of China (NSFC) under Grant No. 10802085.

REFERENCES

1. Shan X, Chen H. Lattice Boltzmann model for simulating flows with multiple phases and components. *Physical Review E* 1993; **47**(3):1815–1819.
2. Martys NS, Chen HD. Simulation of multicomponent fluids in complex three-dimensional geometries by the lattice Boltzmann method. *Physical Review E* 1996; **53**(1):743–750.
3. Inamuro T, Ogata T, Tajima S, Konishi N. A lattice Boltzmann method for incompressible two-phase flows with large density differences. *Journal of Computational Physics* 2004; **198**(2):628–644.
4. Sankaranarayanan K, Shan X, Kevrekidis IG, Sundaresan S. Analysis of drag and virtual mass forces in bubbly suspensions using an implicit formulation of the lattice Boltzmann method. *Journal of Fluid Mechanics* 2002; **452**:61–96.
5. Permnath KN, Abraham J. Lattice Boltzmann simulations of drop-drop interactions in two-phase flows. *International Journal of Modern Physics C* 2005; **16**(1):25–44.
6. Shan X, Doolen G. Multicomponent lattice-Boltzmann model with interparticle interaction. *Journal of Statistical Physics* 1995; **81**:379–393.
7. Kang QJ, Zhang DX, Chen SY. Displacement of a two-dimensional immiscible droplet in a channel. *Physics of Fluids* 2002; **14**(9):3203–3214.
8. Benzi R, Biferale L, Sbragaglia M, Succi S, Toschi F. Mesoscopic modeling of a two-phase flow in the presence of boundaries: the contact angle. *Physical Review E* 2006; **74**(2):021509.
9. Huang HB, Thorne DT, Schaap MG, Sukop M. Proposed approximation for contact angles in Shan-and-Chen-type multicomponent multiphase lattice Boltzmann models. *Physical Review E* 2007; **76**:066701.
10. Raiskinmaki P, Koponen A, Merikoski J, Timonen J. Spreading dynamics of three-dimensional droplets by the lattice Boltzmann method. *Computational Materials Science* 2000; **18**:7–12.
11. Latva-Kokko M, Rothman DH. Static contact angle in lattice Boltzmann models of immiscible fluids. *Physical Review E* 2005; **72**(4):046701.
12. Pan C, Hilpert M, Miller CT. Lattice-Boltzmann simulation of two-phase flow in porous media. *Water Resources Research* 2004; **40**:W01501.
13. Li H, Pan C, MIller CT. Pore-scale investigation of viscous coupling effects for two-phase flow in porous media. *Physical Review E* 2005; **72**:026705.
14. Yiotis AG, Psihogios J, Kainourgiakis ME, Papaioannou A, Stubos AK. A lattice Boltzmann study of viscous coupling effects in immiscible two-phase flow in porous media. *Colloids and Surfaces A*: *Physicochemical and Engineering Aspects* 2007; **300**:35–49.
15. Langaas K, Papatzacos P. Numerical investigations of the steady state relative permeability of a simplified porous medium. *Transport in Porous Media* 2001; **45**:241–266.
16. Sukop M, Huang HB, Lin CL, Deo MD, Oh K, Miller JD. Distribution of multiphase fluids in porous media: comparison between lattice Boltzmann modeling and micro-x-ray tomography. *Physical Review E* 2008; **77**:026710.
17. Gunstensen AK, Rothman DH, Zaleski S, Zanetti G. Lattice Boltzmann model of immiscible fluids. *Physical Review A* 1991; **43**(8):4320–4327.
18. Rothman DH, Keller JM. Immiscible cellular-automaton fluids. *Journal of Statistical Physics* 1988; **52**(3/4): 1119–1127.
19. Swift MR, Osborn WR, Yeomans JM. Lattice Boltzmann simulation of nonideal fluids. *Physical Review Letters* 1995; **75**(5):830–833.
20. He XY, Chen SY, Zhang RY. A lattice Boltzmann scheme for incompressible multiphase flow and its application in simulation of Rayleigh–Taylor instability. *Journal of Computational Physics* 1999; **152**(2):642–663.
21. Lee T, Lin CL. A stable discretization of the lattice Boltzmann equation for simulation of incompressible two-phase flows at high density ratio. *Journal of Computational Physics* 2005; **206**:16–47.
22. Yuan P, Schaefer L. Equations of state in a lattice Boltzmann model. *Physics of Fluids* 2006; **18**:042101.
23. Shan X, Chen H. Simulation of nonideal gases and liquid–gas phase-transitions by the lattice Boltzmann equation. *Physical Review E* 1994; **49**:2941–2948.
24. Avraam DG, Payatakes AC. Generalized relative permeability coefficients during steady-state 2-phase flow in porous media, and correlation with the flow mechanisms. *Transport in Porous Media* 1995; **20**:135–168.

DOI: 10.1002/fld